Supporting Information:

Highly Hydrophilic and Surface Defect-Rich MOF-74-PA15 By Phytic Acid Etching as Robust Catalyst of Oxygen Evolution Reaction

*Xin Deng, Wenjing Shang, Ke Zhang, Yongbing Lou, Jinxi Chen**

School of Chemistry and Chemical Engineering, Jiangsu Engineering Laboratory of Smart Carbon-Rich Materials and Device, Southeast University, Nanjing 211189, PR China

**Corresponding Author, E-mail address: chenjinxi@seu.edu.cn*

1. Calculation formulas

Some data needed to be calculated in the experimental process, and the calculation formulas were as follows:

Overpotential: $\eta=E_{RHE}-1.23V$,

where E_{RHE} referred to reversible hydrogen electrode, $E_{RHE}=E_{Ag/AgCl}+0.059*pH+0.197V$

Tafel slope: $\eta = b \log j + a$,

where b was the Tafel slope. It was derived from the LSV curve, log j (j was the current density) as the abscissa and η as the ordinate, and the resulting slope was called the Tafel slope.

C_{dl} is estimated by plotting $\Delta J=(Ja-Jc)$ at 1.0394 V (vs. RHE) against the scan rates.

2.Materials

Ferrous chloride tetrahydrate ($FeCl_2 \cdot 4H_2O$), 2.5-dihydroxyterephthalic acid (H_4DOBDC), Phytic acid (ca.50% in Water) (Pa) were purchased from Aladdin. Methanol (CH_3OH), Ethanol (C_2H_5OH), Nickel foam (NF), and Ultrapure water (UW) were obtained from the Nanjing Jingge. All chemicals' reagents are analytical grade and were directly used without any further purification process.

3. Characterizations

Powder X-ray diffraction (XRD) was employed to characterise the phases composition. (Ultima IV, using Cu Kα as radiation source (λ = 1.5406 Å), 2θ = 5º-80º). The functional groups were using Fourier transform infrared spectroscopy (FT-IR) (Nicolet 5700). The morphology of the materials was observed using scanning electron microscopy (SEM, Ultra Plus, 1nm @ 15kV) and transmission electron microscopy (TEM, Talos F200X G2, 200 kV). The elemental composition and valence of the samples were determined by X-ray photoelectron spectroscopy (XPS, Thermo fisher Nexsa) with Al Kα radiation source (hν = 1486.6 eV) and foreign carbon (C 1s) with binding energy of 284.0 eV was used as reference standard. The contact angle (CA) instrument (Chengde Dingsheng JY-82C) was employed to evaluate the wettability of the catalysts. N_2 adsorption–desorption isotherms were measured on Micromeritics ASAP 2460 instrument (BET). Electron paramagnetic resonance (EPR) spectra were collected on CIQTEK EPR200-Plus. The Elemental content of MOF-74-PA15 were determined by ICP-MS on an Agilent 7800 (MS) instrument.

4. Pre-treated nickel foam (NF)

All Nickel Foam (NF) utilized as the substrate was ultrasonic cleaned in 3 M HCl for 15 minutes. Subsequently, the NF with the oxide layer removed underwent separate ultrasonic cleaning steps using deionized water and ethanol, each lasting 5 minutes. Following this, the thoroughly cleaned NF was vacuum dried at 60°C for 12 hours.

5. Electrochemical test

Electrochemical tests were carried out at the CHI660D electrochemical workstation on a three-electrode system. In situ loaded NF (1 x 1 cm^2) with the material was acted as working electrode, the Pt electrode (1 x 1 cm^2) as counter electrode and the Ag/AgCl electrode was the reference electrode. At the scan rate of 5 mV s^{-1}, linear sweep voltammetry (LSV) curves were collected. To obtain more reliable and accurate data, all the working electrodes were activated before LSV curves were obtained and all LSV curves were compensated with 95 % *iR*. To avoid the possibility of redox current effects, cyclic voltammetry (CV) curves were run at different scanning rates (20, 40, 60, 80, 100 and 120 mV s^{-1}) in the non-Faraday range (0 V-0.08 V). The ZView application was selected to analyze and fit the electrochemical impedance spectroscopy (EIS) results which were collected under open-circuit voltage conditions. All equations used in this paper are listed in the supporting information.

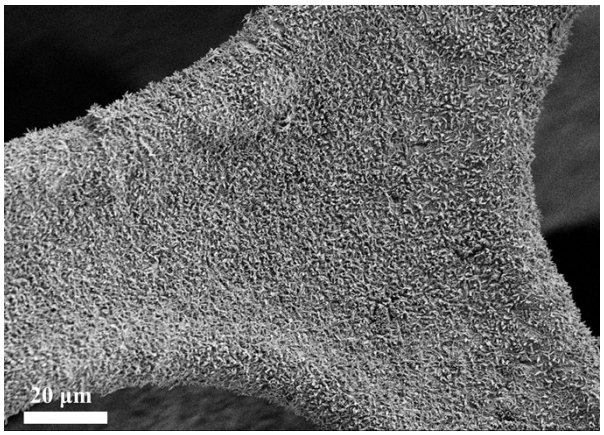

Figure S1. SEM images of MOF-74.

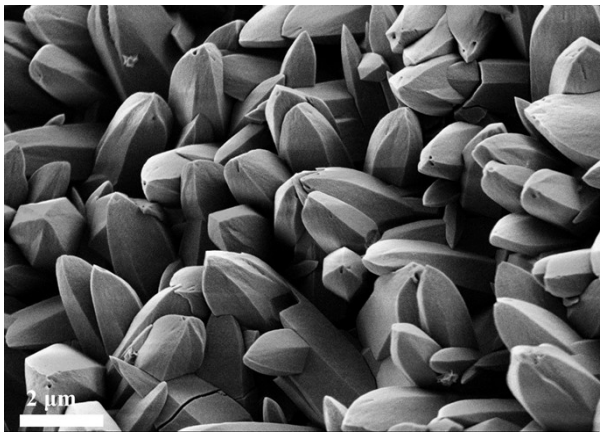

Figure S2. SEM images of MOF-74-PA5.

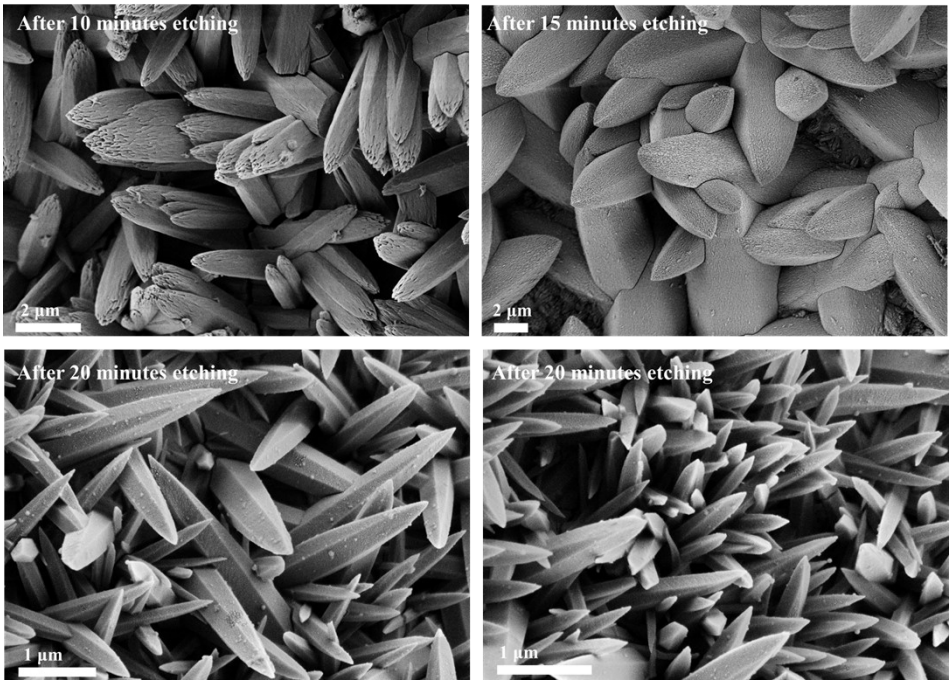

Figure S3. SEM images with different etching times.

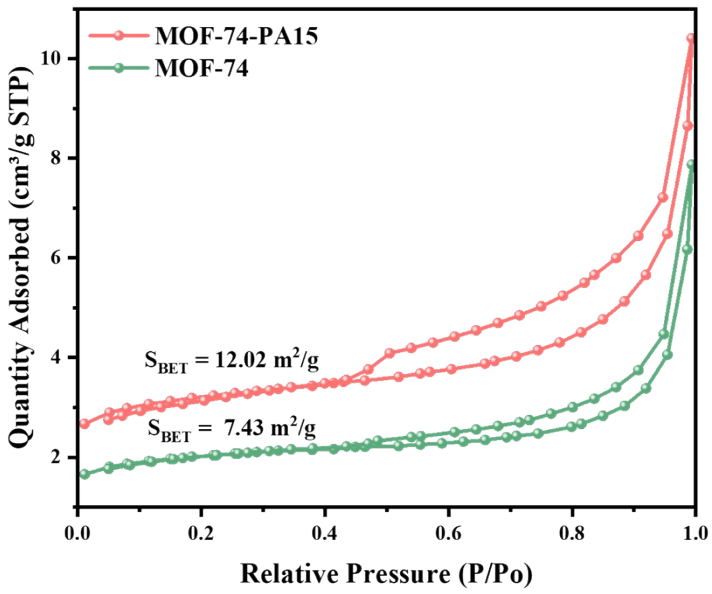

Figure S4. Nitrogen sorption isotherm of MOF-74 and MOF-74-PA15.

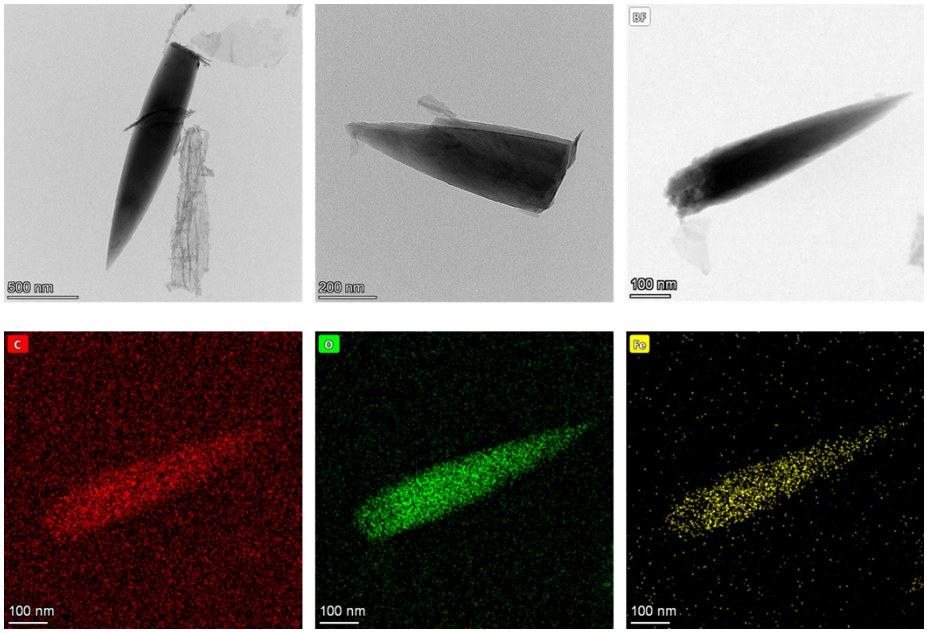

Figure S5. TEM images of MOF-74 and corresponding EDS images.

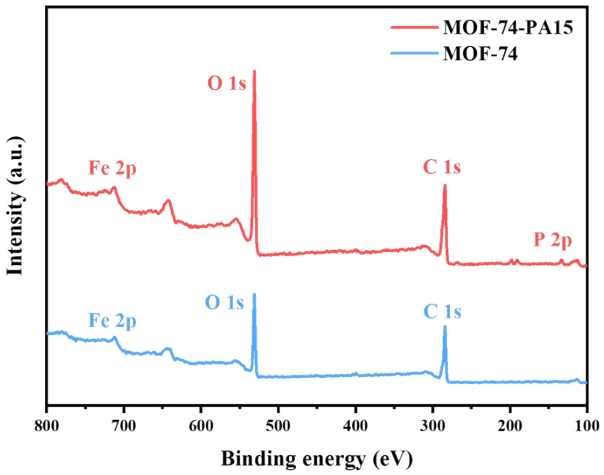

Figure S6. Full survey spectrum of MOF-74 and MOF74-PA15.

Figure S7. EPR spectra spectroscopy of MOF-74 and MOF-74-PA15.

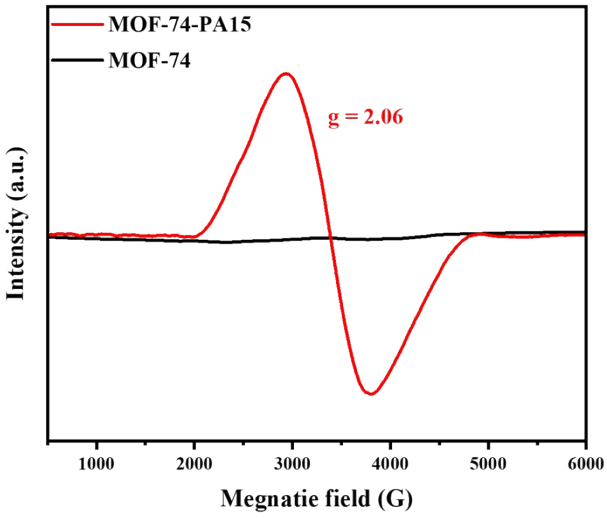

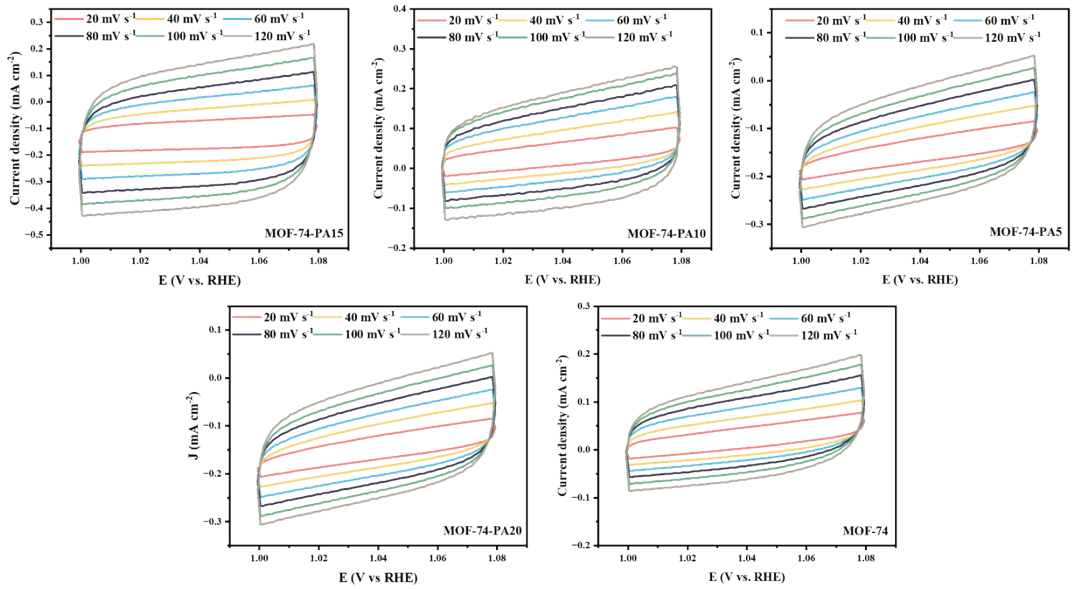

Figure S8. Cyclic voltammetry curves of MOF-74-PA15, MOF-74-PA10, MOF-74-PA5, MOF-74-PA20 and MOF-74.

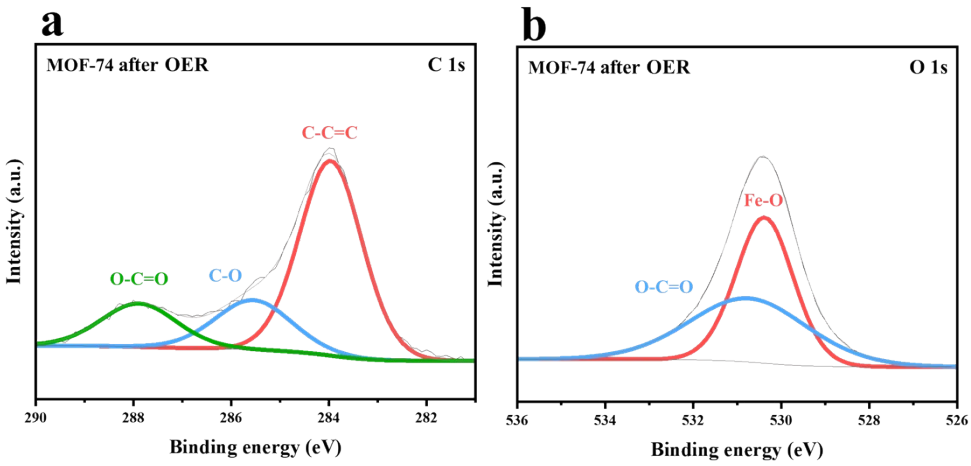

Figure S9. High resolution XPS spectra of MOF-74 after OER. a) C, b) O.

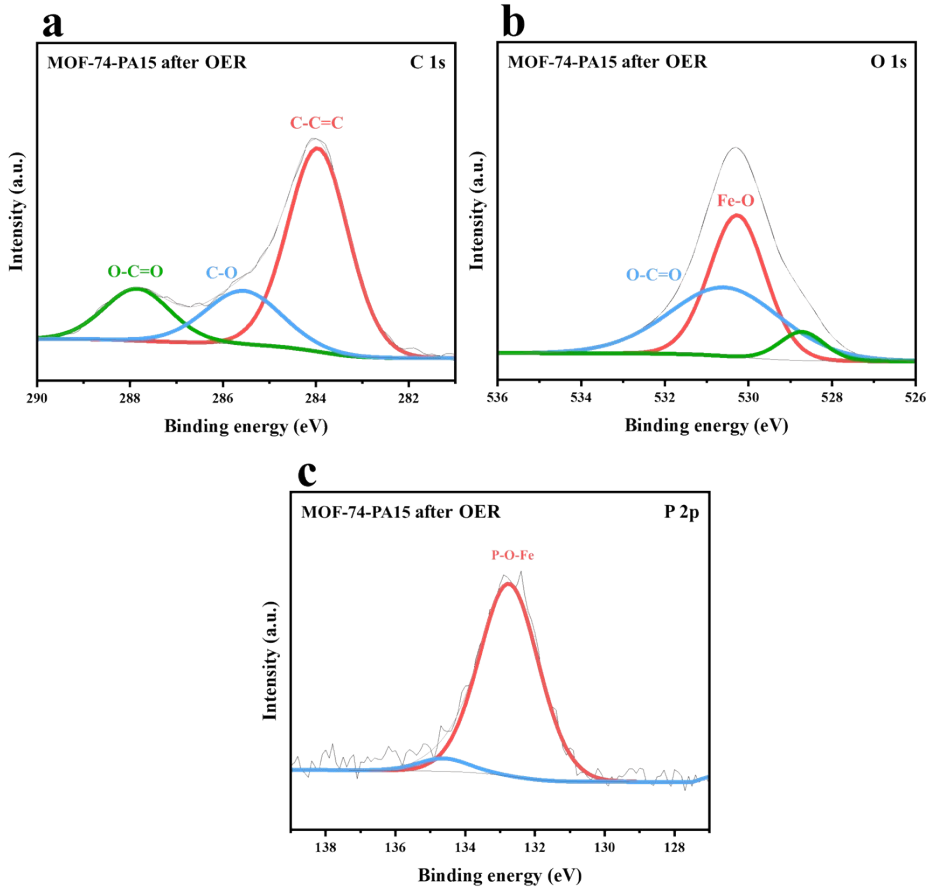

Figure S10. High resolution XPS spectra of MOF-74-PA15 after OER. a) C, b) O, and c) P.

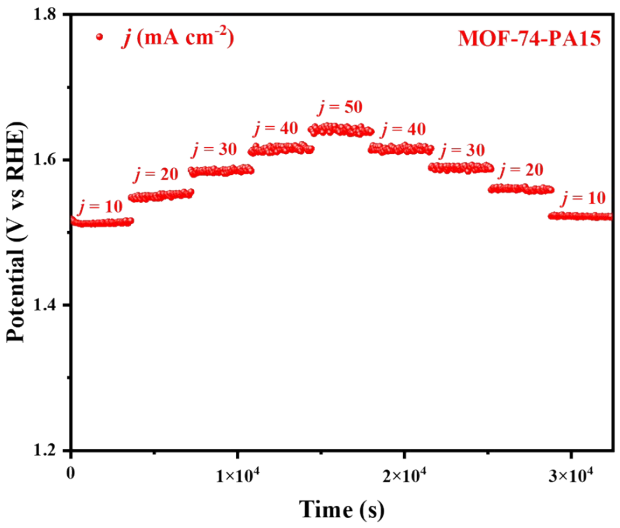

Figure S11. Multistep chronoamperometric curves of MOF-74-PA15.

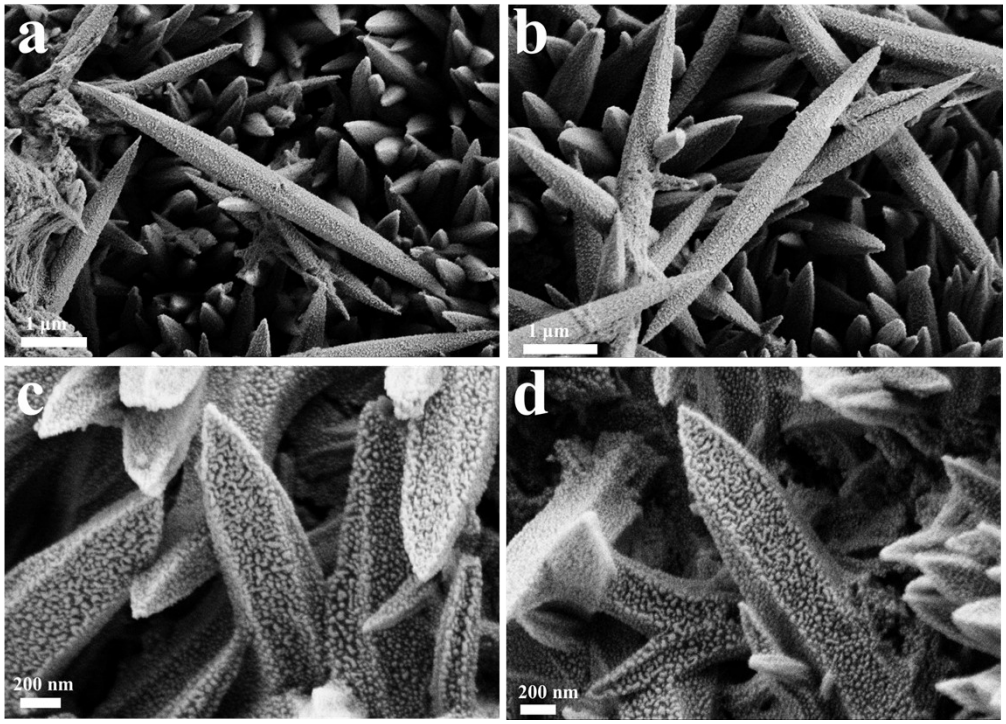

Figure S12. SEM images after OER of a,b) MOF-74 and c,d) MOF-74-PA15.

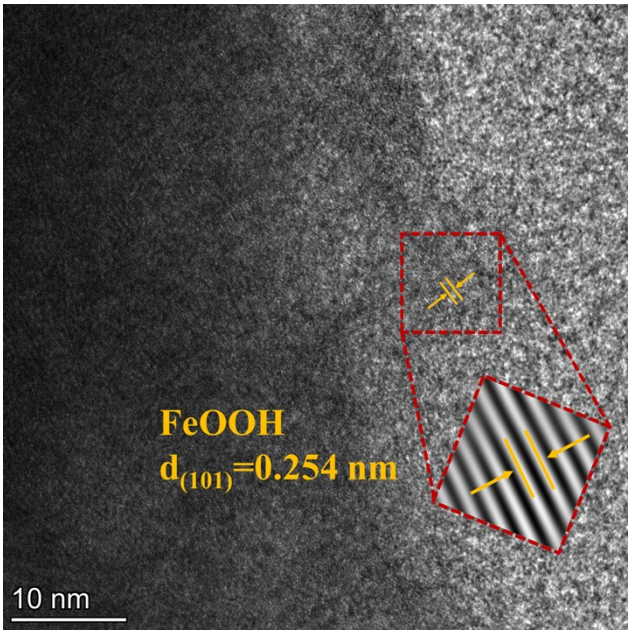

Figure S13. HRTEM images of MOF-74-PA15 after OER.

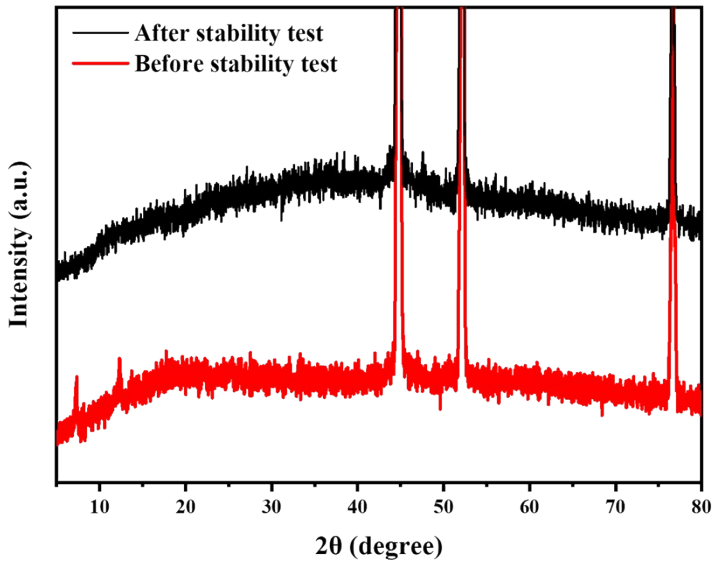

Figure S14. XRD pattern of MOF74-PA15 before and after stability.

Table S1. The contents of Fe and P elements in MOF-74 and MOF-74-PA15 measured by ICP-MS.

Samples	Fe / wt%	P / wt%
MOF-74	16.32	-
MOF-74-PA15	18.52	1.00

Table S2. Comparison of OER catalytic performance of various MOFs.

Catalyst	*Current Density (mA cm^{-2})*	*Overpotential (mV)*	*Reference*
MOF-74-PA15	100	250	This work
UV/O_3-Fe-MOF/NF	100	241	[1]
NiFe-NFF	100	253	[2]
Cu–Fe–NH_2 MOF/NF	100	270	[3]
$FeMn_6Ce_{0.5}$-MOF-74/NF	100	281	[4]
$FeNi_3$-BTC	100	284	[5]
IrO_2/NF	100	550	[1]
Co_3O_4@MOF-74	50	285	[6]
BN-CoFe-MOF	50	314	[7]
CoFe–MOF@Pa	10	203	[8]
F-FeNi-MOFs	10	218	[9]
Fe–CoNi MOFs	10	230	[10]
NiCo/Fe_3O_4/MOF-74	10	238	[11]
Ni_2P/Fe(O)OH-40/NF	10	240	[12]

Reference

1. Z. Wang, J. Xu, J. Yang, Y. Xue and L. Dai, *Chem. Eng. J.*, 2022, **427**, 131498.
2. C. Cao, D. D. Ma, Q. Xu, X. T. Wu and Q. L. Zhu, *Adv. Funct. Mater.*, 2018, **29,** 1807418.
3. N. K. Shrestha, S. A. Patil, S. Cho, Y. Jo, H. Kim and H. Im, *J. Mater. Chem. A*, 2020, **8**, 24408-24418.
4. N. Chai, Y. Kong, T. Liu, S. Ying, Q. Jiang and F.-Y. Yi, *Dalton Trans.*, 2023, **52**, 11601-11610.
5. F. Zheng, Z. Zhang, D. Xiang, P. Li, C. Du, Z. Zhuang, X. Li and W. Chen, *J. Colloid Interface Sci.*, 2019, **555**, 541-547.
6. W. Gao, W. Gou, R. Wei, X. Bu, Y. Ma and J. C. Ho, *Appl. Mater. Today*, 2020, **21,** 100820.
7. L. Shen, X. Zhang, H. He, X. Fan, W. Peng and Y. Li, *J. Colloid Interface Sci.*, 2024, **676**, 238-248.
8. T. Zhao, D. Zhong, G. Hao and Q. Zhao, *Appl. Surf. Sci.*, 2023, **607,** 155079.
9. Y. Hu, Y. Fan, L. Li, J. Zhou, Z. Hu, J. Q. Wang, J. Dong, S. Zhao and L. Zhang, *Small*, 2024, **20,** 2400042.
10. L. Yu, J. Xiao, C. Huang, Z. Zhang, M. Qiu, Y. Yu, Y. Wang and J. C. Yu, *J. Mater. Chem. A*, 2022, **10**, 17552-17560.
11. X. Wang, H. Xiao, A. Li, Z. Li, S. Liu, Q. Zhang, Y. Gong, L. Zheng, Y. Zhu, C. Chen, D. Wang, Q. Peng, L. Gu, X. Han, J. Li and Y. Li, *J. Am. Chem. Soc.*, 2018, **140**, 15336-15341.
12. Y. Xing, S. Liu, Y. Liu, X. Xiao, Y. Li, Z. Wang, Y. Hu, B. Xin, H. Wang and C. Wang, *Nano Energy*, 2024, **123,** 109402.